Eur Radiol (2013) 23:1660–1668
DOI 10.1007/s00330-012-2747-0

HEPATOBILIARY-PANCREAS

Hepatocellular carcinoma and focal nodular hyperplasia of the liver: differentiation with CT spectral imaging

Yixing Yu · Xiaozhu Lin · Kemin Chen · Weimin Chai · Shudong Hu · Rongbiao Tang · Jing Zhang · Lixiu Cao · Fuhua Yan

Received: 13 September 2012 / Revised: 5 November 2012 / Accepted: 19 November 2012 / Published online: 10 January 2013

Abstract
Objectives To investigate the value of CT spectral imaging in differentiating hepatocellular carcinoma (HCC) from focal nodular hyperplasia (FNH) during the arterial phase (AP) and portal venous phase (PP).
Methods Fifty-eight patients with 42 HCCs and 16 FNHs underwent spectral CT during AP and PP. The lesion–liver contrast-to-noise ratio (CNR) at different energy levels, normalised iodine concentrations (NIC) and the lesion–normal parenchyma iodine concentration ratio (LNR) were calculated. The two-sample *t* test compared quantitative parameters. Two readers qualitatively assessed lesion types according to imaging features. Sensitivity and specificity of the qualitative and quantitative studies were compared.
Results In general, CNRs at low energy levels (40–70 keV) were higher than those at high energy levels (80–140 keV). NICs and LNRs for HCC differed significantly from those of FNH: mean NICs were 0.25 mg/mL±0.08 versus 0.42 mg/mL±0.12 in AP and 0.52 mg/mL±0.14 versus 0.86 mg/mL±0.18 in PP. Mean LNRs were 2.97±0.50 versus 6.15±0.62 in AP and 0.99±0.12 versus 1.22±0.26 in PP. NICs and LNRs for HCC were lower than those of FNH. LNR in AP had the highest sensitivity and specificity in differentiating HCC from FNH.
Conclusions CT spectral imaging may help to increase detectability of lesions and accuracy of differentiating HCC from FNH.

Y. Yu · X. Lin · K. Chen (✉) · W. Chai · S. Hu · R. Tang · J. Zhang · L. Cao · F. Yan
Department of Radiology, Ruijin Hospital, Shanghai Jiaotong University School of Medicine, No.197, Rui Jin Er Road, Shanghai, China 200025
e-mail: chenkemin2012@163.com

Key Points
- *CT spectral imaging may help to detect hepatocellular carcinoma* (*HCC*).
- *CT spectral imaging may help differentiate HCC from focal nodular hyperplasia*.
- *Quantitative analysis of iodine concentration provides greater diagnostic confidence*.
- *Treatment can be given with greater confidence*.

Keywords Hepatocellular carcinoma · Focal nodular hyperplasia · Computed tomography · CT spectral imaging · Monochromatic image

Abbreviations

AP	arterial phase
CNR	contrast-to-noise ratio
FNH	focal nodular hyperplasia
GSI	Gemstone Spectral Imaging
HCC	hepatocellular carcinoma
LNR	lesion–normal parenchyma iodine concentration ratio
NIC	normalised iodine concentration
PP	portal venous phase

Introduction

Hepatocellular carcinoma (HCC) is the most common primary liver cancer worldwide and is particularly prominent in Asian and Mediterranean populations [1]. HCC usually occurs as a complication of chronic liver disease and most often arises in cirrhotic livers. The imaging appearance of HCC can vary dramatically. However, focal nodular

hyperplasia (FNH) is the second most common benign liver tumour after haemangioma [2]. It is characterised by nodular hyperplasia of the hepatic parenchyma around a central stellate area of fibrosis associated with an anomalous artery [3]. Typical FNH can be diagnosed with confidence by using CT or MR imaging [2–4]. Atypical FNH may show less intense enhancement, unusual appearance or non-enhancement of the central scar and pseudocapsular enhancement on delayed images [2]. In these cases, it may be difficult to differentiate between atypical FNH and HCC [5]. Differentiation between HCC and FNH is essential because of different therapeutic approaches. Liver resection has been shown to be a highly effective treatment technique in patients with HCC; conversely, an observational approach is justified in patients with FNH [6].

Recently a dual energy spectral CT imaging mode based on the rapid switching between high and low energy data sets from view to view was introduced to produce both the material decomposition images and monochromatic spectral images at energy levels ranging from 40 to 140 keV [7]. This imaging method has also found use in several clinical applications including preoperative detection of insulinomas [7], differentiating hypervascular hepatic lesions [8] and diagnosis of pulmonary embolism [9]. The purpose of this study was to preliminarily investigate the usefulness of CT spectral imaging in differentiating HCC from FNH.

Materials and methods

Patients

The ethics committee at our institution (Ruijin Hospital) approved this prospective study and all patients provided written informed consent. From June 2010 to June 2012, 228 patients (145 men, 83 women; median age 56 [16–76 years]) known to have or suspected of having hypervascular liver tumours underwent dual-phase CT imaging in the spectral imaging mode on a High Definition CT system (Discovery CT750HD, GE Healthcare, USA). A total of 170 patients were excluded from the study because (a) they had no HCC or FNH or (b) there was inadequate confirmation of histological findings. Therefore 58 patients (37 men, 21 women; median age 45 [16–72 years]) were included in our study. Forty-two patients (34 men, 8 women; median age 58 [45–72 years]) had 42 HCCs (mean diameter 3.8 cm, 1.2–7.6 cm) and 16 patients (3 men, 13 women; median age 32 [16–49 years]) had 16 FNHs (mean diameter 4.0 cm, 2.0–8.2 cm). Ten of 42 HCCs were in patients with cirrhosis, all resulting from chronic hepatitis B. All HCCs in 42 patients were proven pathologically after surgical resection. Retrospective analysis of pathologic reports revealed the following grades of differentiation according to Edmondson–Steiner classification: 3 grade 1HCCs, 18 grade 2 HCCs, 17 grade 3 HCCs and 4 grade 4 HCCs. Eight of 16 FNHs were confirmed histologically after biopsy due to diagnostic uncertainty and the rest were proven pathologically after surgical resection because of the misdiagnosis for liver cancer.

CT examinations

Unenhanced and two-phase contrast material enhanced CT examinations were performed by using the Discovery CT750 HD CT system (64 detectors). All patients underwent imaging craniocaudally in the supine position. Unenhanced images were acquired following scout imaging with the conventional helical mode at a tube voltage of 120 kVp. Patients were then injected with a total of 80–100 mL non-ionic contrast medium (iopamidol, Iopamiro 300; Shanghai BRACCO Sine Pharmaceutical, China) via antecubital venous access by using a power injector (Ulrich medical, Germany) at a rate of 3–4 mL/s during the arterial (AP) and portal venous phase (PP). The imaging delay for AP imaging was determined using automatic image-triggering software (SmartPrep; GE Healthcare). AP imaging began 8 s after the trigger attenuation threshold (100 HU) was reached at the level of the supra-coeliac abdominal aorta. At a delay of 30 s after AP imaging, PP imaging began.

Arterial phase and portal venous phase imaging were performed in the spectral imaging mode with fast tube voltage switching between 80 and 140 kVp on adjacent views during a single rotation. Other imaging parameters were as follows: collimation thickness 0.625 mm, tube current 600 mA, rotation speed 0.6 s, helical pitch 0.983, CT dose index volume 21.8 mGy (comparable to 21.5-mGy dose administered for conventional contrast-enhanced liver imaging in a normal-size patient at our institution). The CT images were reconstructed by using projection-based material-decomposition software and a standard reconstruction kernel. Three types of images were reconstructed from the single spectral CT acquisition for analysis: conventional polychromatic images obtained at 140 kVp, iodine-and water-based material decomposition images, and monochromatic images obtained at values ranging from 40 to 140 keV.

Quantitative analyses

All the measurements were performed on an advanced workstation (AW4.4; GE Healthcare, Waukesha, WI, USA) with the Gemstone Spectral Imaging (GSI) viewer. The default 70-keV monochromatic images and iodine-based material decomposition images were reviewed. Circular or elliptical regions of interest (ROIs) were placed in the lesions, normal hepatic parenchyma and aorta on the default 70-keV monochromatic images. The ROIs encompassed as much of the high-enhancing areas of the lesions as

possible. Areas of focal change in hepatic parenchymal attenuation, large vessels, and prominent artefacts were avoided carefully. To ensure consistency, all measurements were performed three times at different image levels, and average values were calculated. For all measurements, the size, shape and position of the ROIs were kept consistent between the two phases by applying the copy-and-paste function. The GSI viewer software package automatically calculated the CT values, iodine (water), water (iodine), fat (calcium) and calcium (fat) concentration for the lesions and normal hepatic parenchyma. Three recently introduced parameters were derived from the CT values and iodine concentration measurements: (a) contrast-to-noise ratio (CNR) at different energy levels (40–140 keV, interval 10 keV), calculated as $CNR=(CT_{lesion}-CT_{liver})/SD_{noise}$, where CT_{lesion} and CT_{liver} are the CT values in the lesions and in the normal hepatic parenchyma and SD_{noise} is the standard deviation for CT values of the normal parenchyma as background; (b) normalised iodine concentration (NIC), calculated as $NIC=IC_{lesion}/IC_{aorta}$, where IC_{lesion} and IC_{aorta} are the iodine concentrations in the lesions and in the aorta; iodine concentrations in the lesions were normalised to those of the aorta in order to minimise variations in patients. (c) The lesion-to-normal parenchyma ratio (LNR) for the iodine concentration, calculated as $LNR=IC_{lesion}/IC_{liver}$, where IC_{lesion} and IC_{liver} are the iodine concentrations in the lesions and in the normal hepatic parenchyma.

Qualitative analyses

The two radiologists (each with more than 15 years' experience) qualitatively reviewed the CT images including conventional polychromatic images, monochromatic images and iodine-based material decomposition images with the GSI viewer in consensus at a workstation (AW4.4; GE Healthcare). They were blinded to the diagnosis of the lesion, the patient information and the results of the correlative imaging examinations. The readers recorded the following lesion features: number, density, necrosis, calcification, pseudocapsule, fatty metamorphosis, central scars, presence of feeding vessels and enhancement pattern. For the detectability of each set of images, the true number of lesions in each image set was evaluated by comparing them with standard-of-reference findings. The relative density of the lesion with respect to the hepatic parenchyma was recorded as one of four grades: hypodensity, isodensity, hyperdensity or mixed. The enhancement pattern was described as homogeneous or heterogeneous. The changes in enhancement degree or pattern between the two phases were characterised as expansion, washout or none. Expansion was defined as an increasing area of enhancement in the lesion, whereas washout was defined as a change from high density relative to the density of the liver during the AP to isodensity or hypodensity relative to that of the liver during the PP.

Finally, the readers in consensus characterised each lesion as an HCC or FNH on the basis of the imaging findings. The typical enhancement pattern for HCC consisted of a large, rapid enhancement in the AP with a relatively quick washout in the PP, which was often called "quick in and quick out". FNH usually presented as a homogeneous, well-defined, hypervascular lesion with a characteristic central scar in the AP and became isodense or slightly hyperdensity in the PP. Differences among the observers were resolved by means of consensus conference. The sensitivity (correct diagnoses of HCC) and specificity (correct diagnoses of FNH) of the individual phase were evaluated.

Statistical analysis

The data were analysed using SPSS13.0 (Chicago, IL, USA). Quantitative values were recorded as mean ± standard deviation. The two-sample *t* test was performed to compare the quantitative parameters CNR, NIC and LNR between the HCC and FNH, with $P<0.05$ indicating significance.

Receiver operating characteristic (ROC) curves were generated to help establish the threshold values of NIC and LNR required for significant differentiation of HCC from FNH. The diagnostic capability was determined by calculating the area under the ROC curve. The best sensitivity and specificity were achieved by using the optimal thresholds. Sensitivity was defined as the number of correct diagnoses of HCC divided by the number of proven HCC, multiplied by 100. Specificity was defined as the number of correct diagnoses of FNH divided by the number of proven FNH, multiplied by 100. The null hypothesis test was that the area under the ROC curve was 0.5; the alternative was that this area was greater than 0.5. The McNemar test was used to test for the statistical differences in sensitivity and specificity between spectral quantitative image analysis and conventional qualitative image analysis for differentiating HCC from FNH.

Results

Quantitative analyses

The lesion–liver CNR for HCC and FNH at different energy levels (40–140 keV, interval 10 keV) showed certain regularity (Table 1, Figs. 1 and 2). In general, the lesion–liver CNRs at low energy levels (40–70 keV) were higher than those at high energy levels (80–140 keV). The optimal CNR for HCC and FNH could be obtained at 50 keV and 50 keV,

Table 1 Lesion–liver contrast-to-noise ratio (CNR) at the different energy levels (40–140 keV, interval 10 keV)

Group	Number	40 keV	50 keV	60 keV	70 keV	80 keV
AP						
HCC	42	3.21±1.01	3.60±1.13	2.96±1.02	2.70±0.77	1.22±0.11
FNH	16	7.68±1.24	8.30±1.65	7.43±1.60	6.75±1.06	4.08±0.49
P value		<0.001	<0.001	<0.001	<0.001	<0.001
PP		40 keV	50 keV	60 keV	70 keV	80 keV
HCC	42	0.98±0.18	1.25±0.18	1.35±0.18	1.79±0.22	1.26±0.13
FNH	16	1.04±0.18	1.06±0.19	0.87±0.16	0.77±0.12	0.53±0.16
P value		0.766	0.392	0.054	<0.001	<0.001
AP	90 keV	100 keV	110 keV	120 keV	130 keV	140 keV
HCC	0.61±0.13	0.44±0.16	0.42±0.14	0.28±0.17	0.30±0.15	0.31±0.17
FNH	2.31±0.21	1.72±0.25	1.25±0.12	0.98±0.19	0.74±0.10	0.54±0.10
P value	<0.001	<0.001	<0.001	<0.001	<0.001	0.008
PP	90 keV	100 keV	110 keV	120 keV	130 keV	140 keV
HCC	0.95±0.18	0.92±0.13	0.90±0.21	0.88±0.18	0.87±0.19	0.87±0.18
FNH	0.35±0.07	0.25±0.12	0.29±0.12	0.33±0.13	0.35±0.18	0.37±0.13
P value	<0.001	<0.001	<0.001	<0.001	<0.001	<0.001

With the exception of *P* values, data are mean values ± standard deviations. $P<0.05$ indicates a statistically significant difference between HCC and FNH

AP arterial phase, *HCC* hepatocellular carcinoma, *FNH* focal nodular hyperplasia, *PP* portal venous phase

respectively, during the AP and 70 keV and 50 keV, respectively, during the PP. There were significant differences in the optimal CNR between the patients with HCC and the patients with FNH during both the AP (mean optimal CNR, 3.60±1.13 vs 8.30±1.65; $P=0.008$) and the PP (mean optimal CNR, 1.79±0.22 vs 1.06±0.19; $P=0.039$) (Table 1).

Values for the defined quantitative parameters (NIC and LNR) measured in the patients with HCC and in those with FNH are compared in Table 2. There were significant differences in NIC between the patients with HCC and the patients with FNH during both the AP (mean NIC, 0.25 mg/mL±0.08 vs. 0.42 mg/mL±0.12; $P=0.005$) and the PP (mean NIC, 0.52 mg/mL±0.14 vs. 0.86 mg/mL±0.18; $P<0.001$). The patients with FNH had significantly higher LNR than did the patients with HCC during the AP (mean LNR, 6.15±0.62 vs. 2.97±0.50; $P<0.001$) and the PP (mean LNR, 1.22±0.26 vs. 0.99±0.12; $P=0.003$) (Table 2). The fat (calcium) concentrations in patients with HCC were higher than those of patients with FNH. The differences were significant. There were no significant differences in the water (iodine) concentration during the AP and PP between HCC and FNH ($P>0.05$).

The ROC curves of different parameters for differentiating HCC from FNH are shown in Fig. 3. All the ROCs for all parameters were above the reference line.

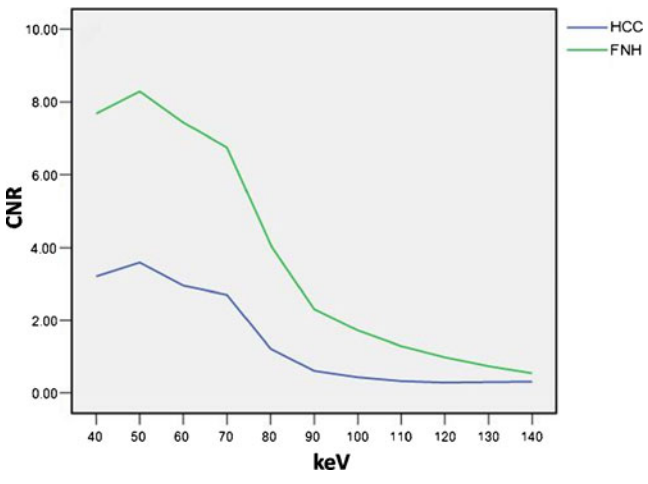

Fig. 1 Lesion–liver contrast-to-noise ratio (CNR) for hepatocellular carcinoma (HCC) and focal nodular hyperplasia (FNH) at the different energy levels (40–140 keV, interval 10 keV) in the arterial phase (AP). CNR values peaked at 50 keV and 50 keV, respectively, during the AP

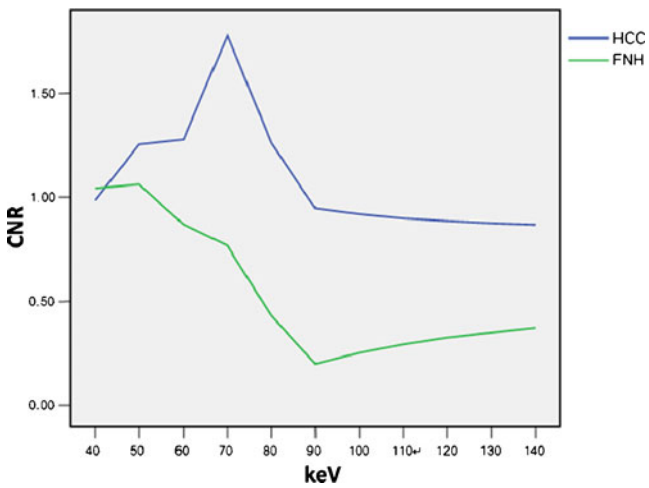

Fig. 2 Lesion–liver CNR for HCC and FNH at the different energy levels (40–140 keV, interval 10 keV) in the portal venous phase (PP). CNR values peaked at 70 keV and 50 keV, respectively, during the PP

Table 2 Quantitative assessment of HCC and FNH with CT spectral imaging

Group	NIC	LNR	Water (iodine)	Fat (calcium)	Calcium (fat)
AP					
HCC	0.25±0.08	2.97±0.50	1,047±8	1,009±11	47±6
FNH	0.42±0.12	6.15±0.62	1,041±4	985±13	76±20
t value	−3.196	−12.911	2.024	4.804	−5.860
P value	0.005	<0.001	0.052	0.004	<0.001
PP					
HCC	0.52±0.14	0.99±0.12	1,042±9	1,003±12	48±8
FNH	0.86±0.18	1.22±0.26	1,042±5	992±3	66±3
t value	−6.518	−3.260	−0.004	3.800	−8.903
P value	<0.001	0.003	0.997	0.001	<0.001

NIC, water (iodine), fat (calcium) and calcium (fat) are in milligrams per millilitre. With the exception of *P* values, data are mean values ± standard deviations. $P<0.05$ indicates a statistically significant difference between HCC and FNH

NIC normal iodine concentration, *LNR* lesion–normal parenchyma iodine concentration ratio

The areas for the LNR (1.00) during the AP were greater than those for other quantitative parameters for differentiating HCC from FNH (Table 3). By using the ROCs, we determined the parameter threshold values required to optimise both the sensitivity and the specificity for differentiating HCC from FNH (Table 3). For example, during the AP, a threshold NIC of 0.24 mg/mL would yield a sensitivity and specificity of 60 % (25 of 42 HCCs) and 100 % (all 16 FNHs), respectively, for differentiating HCC from FNH. However, a threshold LNR of 4.33 would increase the sensitivity and specificity to 100 % (all 42 HCCs) and 100 % (all 16 FNHs), respectively, during the AP.

Qualitative analyses

The detectability of HCCs or FNHs on each imaging set at the consensus reading was as follows: 40 (95 %) of the 42 HCC lesions and all (100 %) of the 16 FNH lesions were detected on conventional polychromatic images. Two HCCs were missed on conventional polychromatic images but could be detected on 70-keV monochromatic images and iodine-based material images (Fig. 4). Thus, all of the HCCs and FNHs were detected on 70-keV monochromatic images or iodine-based material decomposition images. Therefore, the 70-keV monochromatic images or iodine-based material decomposition images showed a higher detectability than conventional polychromatic images.

Qualitative analysis (Table 4) with conventional CT methods showed that necrosis was present in 8 (19 %) of the 42 HCCs and in none of the FNHs (0 %). Neither in HCCs nor in FNHs was calcification present (0 %). Central scars were detected in 10 (63 %) of the 16 FNHs and in none of the HCCs (0 %). Feeding vessels originating from the right or left hepatic artery could be detected in 15 (36 %) of the 42 HCC lesions and in 7 (44 %) of the 16 FNH lesions (Fig. 5a, b). Pseudocapsule was noted in 12 (29 %) of the 42 HCCs and in 2 (13 %) of the 16 FNHs (Fig. 5c, d). Fatty

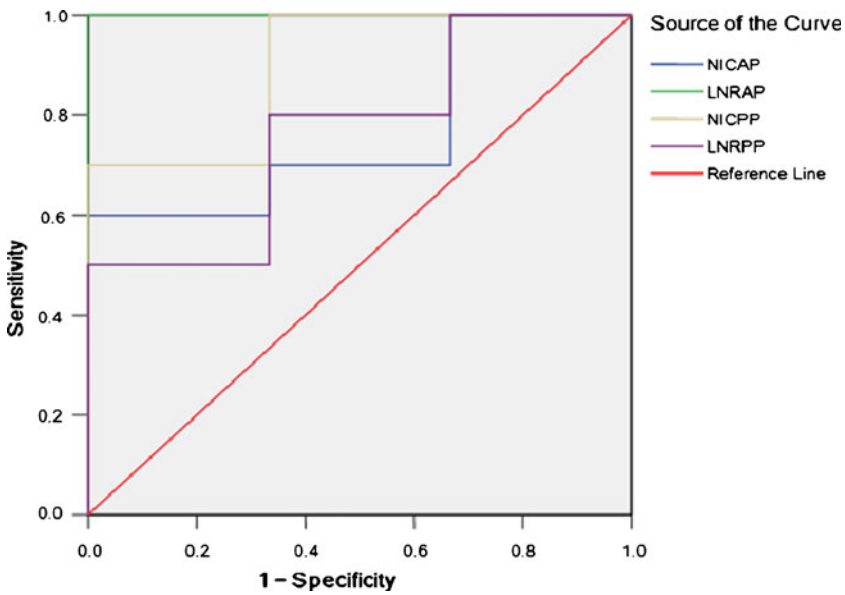

Fig. 3 Receiver operating characteristic curves for normalised iodine concentration (NIC) and lesion–normal parenchyma iodine concentration ratio (LNR) in differentiating HCC from FNH during the AP and PP

Table 3 Areas under the ROC, thresholds, sensitivities and specificities for distinguishing HCC from FNH

Group	NICAP	LNRAP	NICPP	LNRPP
Areas under the ROC	0.767	1.000	0.900	0.767
Thresholds[a]	0.24	4.33	0.58	0.93
Sensitivities[b]	60 (25)	100 (42)	71 (30)	50 (21)
Specificities[c]	100 (16)	100 (16)	100 (16)	100 (16)

NICAP normalised iodine concentrations in the arterial phase, *LNRAP* the lesion–normal parenchyma iodine concentration ratio in the arterial phase, *NICPP* normalised iodine concentrations in the portal venous phase, *LNRPP* the lesion–normal parenchyma iodine concentration ratio in the portal venous phase

[a] Threshold NICAP and NICPP are in milligrams per millilitre

[b] Sensitivity values are percentages. Data in parentheses are numbers of HCC lesions (n=42) used to calculate percentages

[c] Specificity values are percentages. Data in parentheses are numbers of FNH lesions (n=16) used to calculate percentages

metamorphosis was observed in 2 (5 %) of the 42 HCC lesions and none of the FNHs (0 %).

In the unenhanced phase, 28 (67 %) of the 42 HCC lesions were hypodense, 6 (14 %) isodense and 8 (19 %) mixed, whereas 11 (69 %) of 16 FNH lesions were hypodense, 5 (31 %) isodense and 0 % hyperdense compared with the liver parenchyma. Hyperdensity was observed in 34 (81 %) and mixed in 8 (19 %) of the 42 HCC lesions during the AP and hypodensity in 26 (62 %), isodensity in 6 (14 %), hyperdensity in 2 (5 %) and mixed in 8 (19 %) during the PP. However, all (100 %) of the 16 FNH lesions were hyperdense during the AP and 11 (69 %) isodense and 5 (31 %) hyperdense during the PP. Homogeneous enhancement was noted in 28 (67 %) of the 42 HCC lesions and 12 (75 %) of the 16 FNH lesions during the AP and in 28 (67 %) and 15 (94 %), respectively, during the PP. Expansion of enhancement areas between the AP and the PP was observed in neither the HCCs nor the FNHs. Washout was noted in 32 (76 %) of the 42 HCC lesions and 11 (69 %) of the 16 FNH lesions. No enhancement between the AP and the PP was noted in 10 (24 %) of the 42 HCC lesions and 5 (31 %) of the 16 FNH lesions.

In the qualitative analysis of imaging features seen during the combined AP and PP, we achieved sensitivity and specificity of 83 % (35 of 42 HCCs) and 81 % (13 of 16 FNHs), respectively, for differentiating between HCC and FNH. In conclusion, quantitative image analysis with CT spectral imaging, compared with conventional qualitative CT image analysis, improved sensitivity and specificity from 83 % and 81 %, respectively, to 100 % and 100 %, respectively. There were significant differences in sensitivity (P=0.016) but no significant differences in specificity (P=0.250) between spectral quantitative image analysis and conventional qualitative image analysis for differentiating HCC from FNH.

Discussion

The diagnosis of HCC and FNH can usually be based on their different imaging characteristics. These characteristics can be analysed by different diagnostic techniques, such as angiography, CT, Doppler ultrasound and MR imaging. In previous studies [2–4], the role of CT in the diagnosis of HCC and FNH has been discussed, but most studies were primarily focused on analysing the imaging features of the lesions qualitatively [2, 4]; few paid attention to quantitative study. Ruppert-Kohlmayr et al. [3] reported that conventional helical CT combined with quantitative evaluation offered the possibility of detecting differences in liver lesions that were visually similar on CT. However, the quantitative evaluation was based on conventional CT. Our study investigated the application value of quantitative and qualitative analysis with CT spectral imaging in differentiating HCC from FNH.

The averaging attenuation effect of polychromatic X-rays in conventional CT reduces the low-contrast spatial resolution between materials [8]. However, CT spectral imaging can yield monochromatic images at energy levels ranging from 40 to 140 keV, which eliminate the averaging attenuation effects [7]. This would facilitate increasing contrast spatial resolution. The optimal monochromatic images obtained at optimal keV markedly improved lesion-to-liver contrast-to-noise ratio. As was shown in our study, the 70-keV monochromatic images showed a higher detectability of HCCs than conventional polychromatic images. A similar finding was also reported by Lv et al. [10] who found that monochromatic images at energy levels of 40–70 keV could increase detectability in small HCC compared to conventional polychromatic images.

For medical diagnostic imaging, water and iodine are often selected as the basis pair for material decomposition

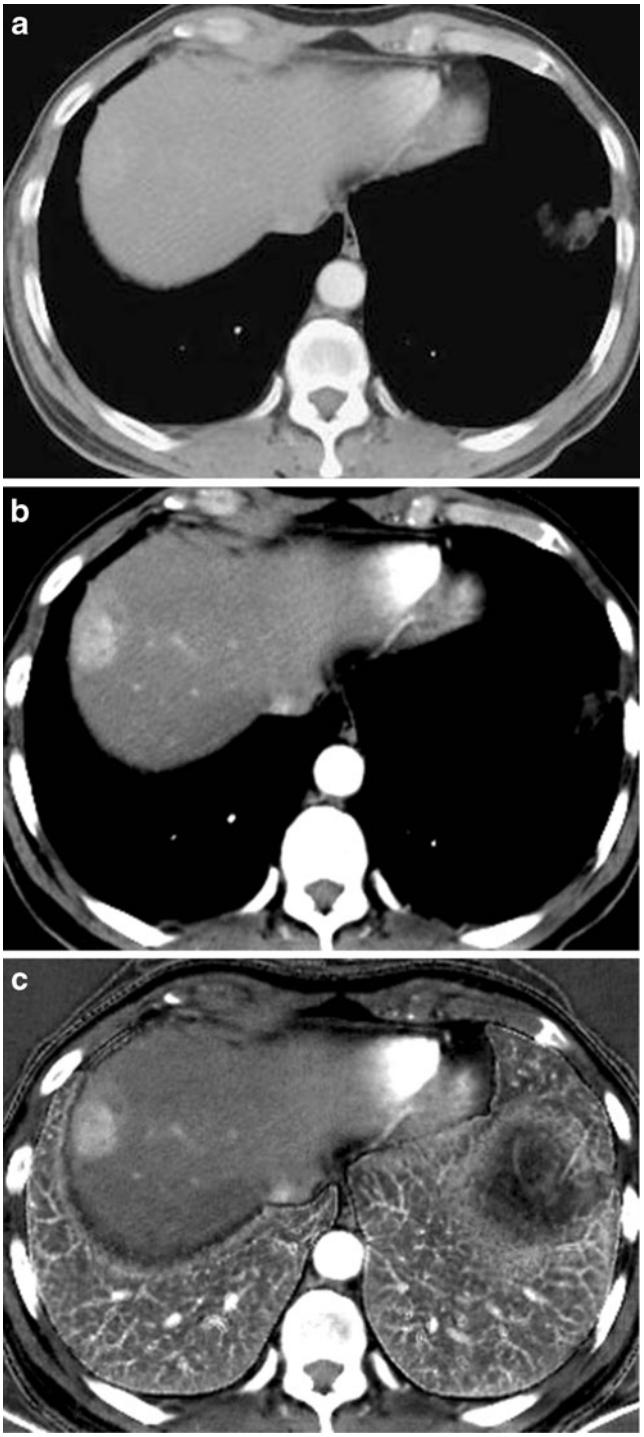

Fig. 4 A 58-year-old man with a 2.5-cm HCC in the hepatic subcapsule. (**a**) Conventional polychromatic image in the AP did not show the lesion clearly. (**b**) Optimal monochromatic image at 70 keV in the AP and (**c**) iodine-based material decomposition image clearly showed a focally hyperattenuating lesion

image presentation because their atomic numbers span the range of atomic numbers for materials generally found in medical imaging and approximate those of soft tissue and iodinated contrast material to result in material attenuation images that are intuitive to interpret [8]. For the hypervascular liver lesions, such as HCC, hepatic haemangioma and FNH, iodine-based material decomposition images could be very sensitive, showing focal uptake of the iodinated contrast material. As was shown in our study, the iodine-based material decomposition images showed a higher detectability of HCCs than conventional polychromatic images. Furthermore, the measured iodine concentration in lesions might be a useful quantitative parameter that reflects the blood supply of lesions.

According to our study results, the lesion–liver CNRs at low energy levels (40–70 keV) were higher than those at high energy levels (80–140 keV). This might be interpreted as the tissue contrast in high energy images being generally small and tissue contrast in low energy images being generally large [11]. The best lesion–liver CNR could be acquired in optimal monochromatic images that were helpful for lesion detection. The iodine concentration in enhancing FNHs was higher than that in enhancing HCCs, during both the AP and the PP. Also, the LNRs for FNHs were higher than those for HCCs; the differences were significant. The obvious enhancement of FNHs seemed to be exclusively caused by arterial vascularisation in the lesion from a feeding artery in the central scar, an

Table 4 Qualitative assessment of HCC and FNH during AP and PP

Features	HCC (n=42)		FNH (n=16)	
	AP	PP	AP	PP
Density				
Hypodensity	0	26 (62)	0	0
Isodensity	0	6 (14)	0	11 (69)
Hyperdensity	34 (81)	2 (5)	16 (100)	5 (31)
Mixed	8 (19)	8 (19)	0	0
Necrosis	8 (19)		0	
Calcification	0		0	
Central scars	0		10 (63)	
Presence of feeding vessels	15 (36)	0	7 (44)	0
Pseudocapsule	12 (29)		2 (13)	
Fatty metamorphosis	2 (5)		0	
Enhancement pattern				
Homogeneous	28 (67)	28 (67)	12 (75)	15 (94)
Heterogeneous	14 (33)	14 (33)	4 (25)	1 (6)
Enhancement change between AP and PP				
Expansion	0		0	
Washout	32 (76)		11 (69)	
None	10 (24)		5 (31)	

Data are numbers of lesions, with percentages in parentheses

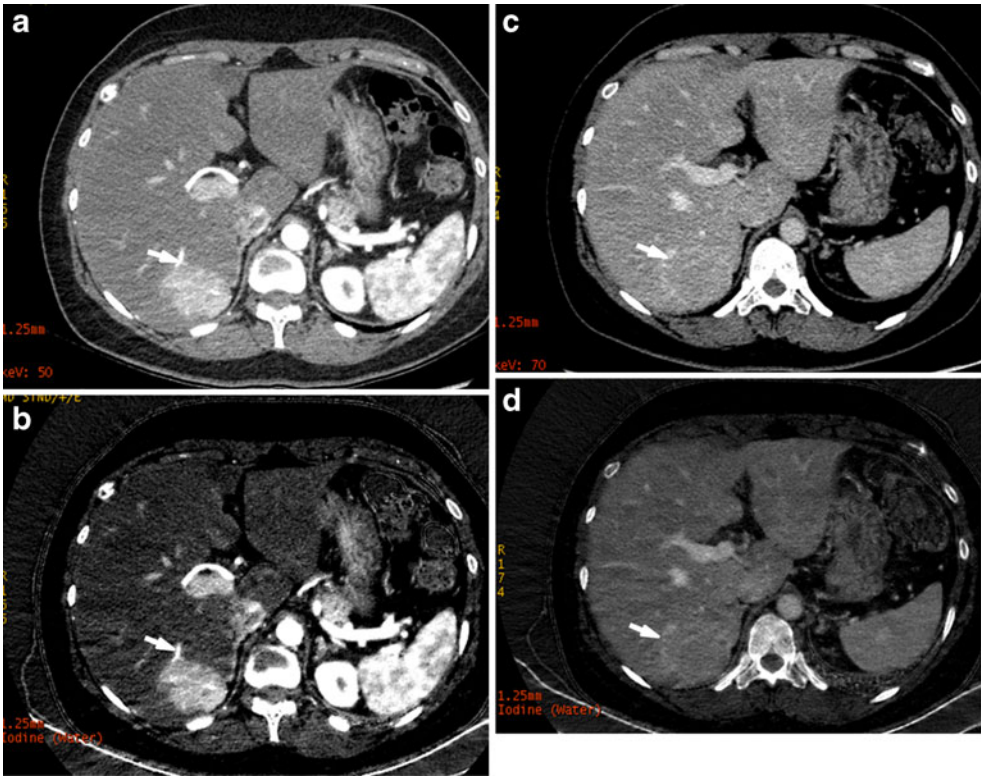

Fig. 5 A 49-year-old woman with a 3.4-cm FNH in the right posterior lobe of the liver. (**a**) Monochromatic image at 50 keV in the AP and (**b**) iodine-based material decomposition image in the AP showed the feeding artery (*arrow*) on the edge of the lesion. (**c**) Monochromatic image at 70 keV in the PP and (**d**) iodine-based material decomposition image in the PP showed the lesion with visible pseudocapsule (*arrow*)

absent capillary bed and a high a rate of centrifugal blood flow [12, 13]. However, according to previous studies, the blood supply types for HCC correlated with pathological grade [14–16]. The number of unpaired arteries increased as the histological grade progressed from well-differentiated HCC to moderately differentiated HCC, but it decreased as the tumour grade progressed from moderately differentiated HCC to poorly differentiated HCC [14]. Some of the poorly differentiated HCCs in our study contained a small number of unpaired arteries, so the iodine concentrations reflecting the blood supply were relatively low. In addition, the measured fat (calcium) concentrations could be used to evaluate the fat content in the lesions. But it was easy to make mistakes in differentiating HCC from FNH only by fat (calcium) concentrations. As shown in our study results, fat (calcium) concentrations in the HCCs were higher than those in the FNHs. There might be two reasons for this. First, small HCC underwent fatty metamorphosis easily [17–19] and the frequency decreased with the increase in tumour diameter [19]. Second, the ROIs were placed in the high-enhancing areas of the lesions which had little fat in our study.

ROC curve analysis in our study revealed that the NIC and the LNR had high specificity for differentiating HCC from FNH. The best quantitative parameter was LNR in AP and the threshold of 4.33 would yield a sensitivity and specificity of 100 % and 100 %, respectively. Compared with conventional qualitative image analysis, quantitative image analysis with spectral CT improved both the sensitivity (from 83 to 100 %) and specificity (from 81 to 100 %). However, the threshold values evaluated in our study were based on the specific populations from which they were obtained and thus were probably overestimations of performance. The accuracy of threshold values needs to be confirmed by a large-sample study in the future.

Our study did have some limitations. Firstly, the results were preliminary and need to be verified by additional studies performed with a larger number of lesions. Secondly, this study focused on differentiating between HCC and FNH. Future investigations with more cases of different types of hypervascular tumours are needed to draw broader conclusions. Thirdly, the HCCs in our study were not classified by pathological grade, because the number of well-differentiated HCC was too small. Finally, as it was not our main purpose, the correlation between the histopathological and CT features was not considered in our study.

In conclusion, CT spectral imaging with monochromatic images, iodine-based material decomposition images and the quantitative iodine concentration analysis may help to increase the detectability of lesions and the accuracy of differentiating HCC from FNH.

Acknowledgements Our work has been supported by the National Natural Science Foundation of China (81071281) and the Science and Technology Commission of Shanghai Municipality (10411953000).

References

1. Schima W, Baron R (2010) Focal liver lesions. In: Hodler J, Von Schulthess GK, Zollikofer Ch L (eds) Diseases of the abdomen and pelvis 2010–2013: diagnostic imaging and interventional techniques, vol XIV. Springer, Milan, pp 63–74
2. Hussain SM, Terkivatan T, Zondervan PE et al (2001) Focal nodular hyperplasia: findings at state-of-the-art MR imaging, US, CT, and pathologic analysis. Radiographics 24:3–17
3. Ruppert-Kohlmayr AJ, Uggowitzer MM, Kugler C, Zebedin D, Schaffler G, Ruppert GS (2001) Focal nodular hyperplasia and hepatocellular adenoma of the liver: differentiation with multiphasic helical CT. Am J Roentgenol 176:1493–1498
4. van den Esschert JW, van Gulik TM, Phoa SSKS (2010) Imaging modalities for focal nodular hyperplasia and hepatocellular adenoma. Dig Surg 27:46–55
5. Savellano DH, Köstler H, Baus S et al (2004) Assessment of sequential enhancement patterns of focal nodular hyperplasia and hepatocellular carcinoma on mangafodipir trisodium enhanced MR imaging. Investig Radiol 39:305–312
6. Langrehr J, Pfitzmann R, Hermann M et al (2006) Hepatocellular carcinoma in association with hepatic focal nodular hyperplasia. Acta Radiologica 47:340–344
7. Lin XZ, Wu ZY, Tao R et al (2012) Dual energy spectral CT imaging of insulinoma–value in preoperative diagnosis compared with conventional multi-detector CT. Eur J Radiol 81:2487–2494
8. Lv P, Lin XZ, Li J, Li W, Chen K (2011) Differentiation of small hepatic hemangioma from small hepatocellular carcinoma: recently introduced spectral CT method. Radiology 259:720–729
9. Geyer LL, Scherr M, Körner M et al (2011) Imaging of acute pulmonary embolism using a dual energy CT system with rapid kVp switching: initial results. Eur J Radiol. doi:10.1016/j.ejrad.2011.02.043
10. Lv P, Lin XZ, Chen K, Gao J (2012) Spectral CT in patients with small HCC: investigation of image quality and diagnostic accuracy. Eur Radiol 22:2117–2124
11. Rutt BK, Cunningham IA, Fenster A (1983) Selective iodine imaging using lanthanum K fluorescence. Med Phys 10:801–808
12. Uggowitzer M, Kugler C, Gröll R et al (1998) Sonographic evaluation of focal nodular hyperplasia (FNH) of the liver with a transpulmonary galactose-based contrast-agent (Levovist). Br J Radiol 71:1026–1032
13. Uggowitzer M, Kugler C, Machan L et al (1997) Power Doppler imaging and evaluation of the resistive index in focal nodular hyperplasia of the liver. Abdom Imaging 22:268–273
14. Asayama Y, Yoshimitsu K, Nishihara Y et al (2008) Arterial blood supply of hepatocellular carcinoma and histologic grading: radiologic-pathologic correlation. AJR Am J Roentgenol 190: W28–W34
15. Hayashi M, Matsui O, Ueda K et al (1999) Correlation between the blood supply and grade of malignancy of hepatocellular nodules associated with liver cirrhosis: evaluation by CT during intraarterial injection of contrast medium. AJR Am J Roentgenol 172:969–976
16. Matsui O (2004) Imaging of multistep human hepatocarcinogenesis by CT during intra-arterial contrast injection. Intervirology 47:271–276
17. Yoshikawa J, Matsui O, Takashima T et al (1988) Fatty metamorphosis in hepatocellular carcinoma: radiologic features in 10 cases. AJR Am J Roentgenol 151:717–720
18. Martin J, Sentis M, Zidan A et al (1995) Fatty metamorphosis of hepatocellular carcinoma: detection with chemical shift gradient-echo MR imaging. Radiology 195:125–130
19. Kutami R, Nakashima Y, Nakashima O, Shiota K, Kojiro M (2000) Pathomorphologic study on the mechanism of fatty change in small hepatocellular carcinoma of humans. J Hepatol 33:282–289